Egypt. J. Chem. **Vol. 68,** SI: Z. M. Nofal, pp. 219 - 225 (2025)

Egyptian Journal of Chemistry

http://ejchem.journals.ekb.eg/

Photocatalytic Performance of Carbon Nanotube/Titanium Dioxide (CNTs/TiO2) Nanocomposites for Ammonium Phosphate Hydrolysis

Mai F.M.Hmamm*[1], Enas Ahmed[1]

[1]*Renewable Energy Science and Engineering Department, Faculty of Postgraduate Studies for Advanced Science, Beni-Suef University, 62511 Beni-Suef, Egypt*

Abstract

This study demonstrates the synthesis of carbon nano tubes (CNTs) /TiO_2 nanocomposites (0–20 wt% CNT) via sol-gel method for photocatalytic hydrogen generation from tri-ammonium phosphate (TAP), a cost-effective and underexplored hydrogen source. Advanced characterization Transmission Electron Microscopy (TEM), X-ray Diffraction (XRD) confirmed the uniform deposition of TiO_2 nanoparticles on multiwalled CNTs, forming heterostructures that facilitate charge separation. Photocatalytic tests revealed a 2.3-fold increase in hydrogen yield at 15 wt% CNT loading compared to pure TiO_2, attributed to CNTs' electron-conducting properties and suppressed charge recombination. The optimal nanocomposite demonstrated a hydrogen generation rate of 28.6 $mmol \cdot h^{-1} \cdot g^{-1}$, underscoring the synergy between CNTs and TiO_2. This work provides a strategy for designing efficient photocatalysts using TAP, a sustainable alternative to conventional hydrogen feedstocks.

Keywords: CNTs/TiO_2 nanocomposites ,tri-ammonium phosphate (TAP)

1. Introduction

Hydrogen holds great promise as a clean energy alternative fuel due to its high energy content per unit mass (142 megajoules per kilogram) and clean combustion, emitting only water vapor[1]. Traditionally, hydrogen production has relied heavily on fossil fuels, with methods like natural gas steam reforming, oil reforming, and coal gasification accounting for the majority of global production, while more sustainable methods like water electrolysis remain limited due to high costs[2-5] . Although renewable techniques such as photocatalysis offer environmentally friendly alternatives, challenges related to efficiency, material cost, and stability persist[5, 6]

Among photocatalytic materials, titanium dioxide, particularly in its anatase phase with a 3.2 electron volt band gap, is widely studied due to its oxidative capabilities and stability [6]. However, its photocatalytic efficiency is hindered by the accelerated collapse of photogenerated hole pairs and by its inability to effectively absorb visible light. Enhancing charge carrier separation and extending photoresponse into the visible spectrum remain central goals for improving titanium dioxide-based systems[7].

To overcome these limitations, numerous studies have investigated the integration of titanium dioxide with conductive carbon-based materials. Among various materials, carbon nanotubes have gained significant interest for their exceptional electrical conductivity, high surface area, and structural compatibility with semiconductor materials[8, 9]. Carbon nanotubes act as electron acceptors or "electron sinks," which helps in promoting the migration of photoexcited electrons away from the titanium dioxide surface, thereby reducing recombination rates and enhancing charge separation [10-13]. The tight connection between titanium dioxide and carbon nanotubes enables the formation of heterojunctions at the interface, which creates a built-in electric field that facilitates more efficient charge transfer[11-13].

Compared to other carbon-based composites such as titanium dioxide/graphene or titanium dioxide/carbon black, titanium dioxide/carbon nanotube composites often show superior photocatalytic performance due to their one-dimensional morphology. Graphene provides an extended two-dimensional plane for charge migration, but it tends to stack during processing, which can hinder dispersion and limit surface accessibility. In contrast, the tubular structure of carbon nanotubes enables better dispersion of titanium dioxide nanoparticles and provides multiple conduction pathways, contributing to improved light absorption, charge separation, and catalytic activity under illumination [12-14].

In parallel with advancements in hydrogen production, efficient and cost-effective hydrogen storage remains a significant challenge. Conventional methods such as high-pressure gas storage and liquefaction are energy-intensive and costly [15]. Solid-state storage using materials like metal hydrides, porous structures such as metal-organic frameworks and layered double hydroxides, and chemical hydrides offers a safer and potentially more efficient alternative [16-19]. Notably,

*Corresponding author e-mail: mai.farg@psas.bsu.edu.eg.; (**Mai F.M.Hmamm**).

Received date 25 February 2025; Revised date 07 May 2025; Accept date 24 May2 025

DOI: 10.21608/EJCHEM.2025.363547.11365

ammonium phosphate compounds have emerged as promising solid-state materials for hydrogen storage are valued for their high hydrogen capacity and release potential under ambient conditions [20-23].
Despite these advances, limited research has focused on coupling photocatalytic systems with solid hydrogen carriers like ammonium phosphate for integrated hydrogen production and release. This study aims to address this gap by investigating the photocatalytic performance of carbon nanotube/titanium dioxide nanocomposites synthesized using the sol–gel method, and their ability to facilitate the degradation of ammonium phosphate for hydrogen gas generation[24-26] .

2. Experimental work

The catalyst was synthesized in two main steps:

2.1. Preparation and Purification of CNTs via the CVD Method

Carbon nanotubes (CNTs) were produced using chemical vapor deposition (CVD), involving the thermal decomposition of acetylene on a Fe-Co/$CaCO_3$ catalyst-supported system. The resulting raw material contained impurities, including metal catalysts (Fe, Co), $CaCO_3$ particles, and amorphous carbon.
To purify the CNTs, 0.05 g of the as-produced material was refluxed in a 3:1 volume ratio of concentrated sulfuric acid to nitric acid at 120 °C for four hours. Once the mixture cooled to room temperature, it was diluted with distilled water and passed through fine-pore filter paper (3 µm) for filtration. Repeated washing with deionized water continued until a neutral pH was achieved. The purified CNTs were then dried at 100 °C. A yield of approximately 68% purified CNTs was obtained from the raw product [27].

2.2. Synthesis of CNTs/TiO_2 Nanocomposites Using a Surfactant-Assisted Sol–Gel Approach

Acid-treated CNTs were incorporated into the TiO_2 matrix using a sol–gel process designed to achieve CNT-to-TiO_2 weight ratios of 5%, 10%, 15%, and 20%. Prior to synthesis, the CNTs were sonicated for one hour to ensure good dispersion, then added to a solution of 2.7 mL distilled water and 27.3 mL isopropanol (total volume: 30 mL).
A titanium precursor solution, prepared by dissolving 3.41 mL of titanium isopropoxide in 18 mL of isopropanol, was mixed in under vigorous stirring to the CNT suspension. The mixture was stirred continuously for 2 hours at room temperature to complete hydrolysis. To control nanoparticle morphology, the solution was optionally aged for 1 hour under static conditions before drying.
The resulting gel was filtered, washed three times with ethanol and distilled water, and then dried at 100 °C for 1.5 hours. The dried nanocomposite was ground into a fine powder and stored in a desiccator. A control TiO_2 sample (without CNTs) was prepared using the same procedure. Crystallization was achieved by sintering all samples at 500 °C for 30 minutes.

3. Characterization Techniques

3.1. Sample analysis

A range of analytical methods was employed to study the properties of the CNTs and their composite materials. To evaluate the crystallinity of the CNTs/TiO_2 composites, powder X-ray diffraction (XRD) analysis was carried out. This was performed using a PANalytical Empyrean diffractometer, equipped with Cu $K\alpha_1$ radiation (λ = 1.5406 Å), operating at an accelerating voltage of 40 kV and a current of 30 mA. The diffraction patterns were recorded over a 2θ interval of 5° to 80°, using a step increment of 0.02°. Transmission electron microscopy (TEM) was used to observe the microstructure, utilizing a JEOL JEM 2010 microscope (JEOL Ltd.) at an operating voltage of 200 kV. For TEM sample preparation, the solids were suspended in ethanol and subjected to ultrasonic treatment for 15 minutes. A drop of the resulting dispersion was then placed on a copper grid and allowed to dry in ambient conditions.

3.2. Catalyst activity tests

The synthesized catalyst was utilized in hydrogen gas production via the hydrolytic decomposition of ammonium phosphate. Hydrolysis of ammonium phosphate was assessed by quantifying hydrogen release through a traditional water-based gas burette apparatus. Before commencing the catalytic reaction, the jacketed reaction flask—fitted with a Teflon-coated magnetic stir bar—was placed on a magnetic stirrer and brought to a temperature of 25 °C. To measure the volume of hydrogen generated, a water-filled burette was joined with the reaction flask. After that, 50 mg of catalyst in 100 mL of aqueous dispersion was put into the reaction flask, and the catalyst solution was stirred at 600 rpm while an estimated weight measured in advance equal to 1 mmol of ammonium phosphate the prepared formulation was incorporated. Every minute, the displacement of the water level was recorded in order to calculate the volume of hydrogen gas evolved. When no hydrogen gas production was seen, the process was stopped. A control experiment was performed under the same conditions but without the addition of any catalytic material, and no noticeable hydrogen gas evolution was observed. This setup was exposed to sunlight during the process (October. 2024 in Beni-Suef city, Egypt).

4. Results and Discussion

4.1.X-ray Diffraction (XRD)

X-ray diffraction (XRD) was employed to investigate the crystalline phases present in the synthesized CNTs/TiO_2 nanocomposites. The XRD pattern, shown in Figure 1, reveals several distinct peaks corresponding to the anatase phase of titanium dioxide. The sharp and well-defined peaks at 2θ values of 25.2°, 37.9°, 48.3°, 53.0°, 55.1°, 62.4°, 68.7°, and 75.0° are attributed to the (101), (103), (200), (105), (213), (116), (220), and (215) planes of anataseTiO_2, respectively, in agreement

with standard (JCPDS card no. 21-1272). These results confirm the successful formation of the anatase crystalline structure.To further characterize the material, the average crystallite size of anataseTiO_2 was estimated using the Scherrer equation:

$$D = \frac{K\lambda}{\beta cos\theta} \quad (1)$$

Where: D is the crystallite size, K is the shape factor (typically 0.9), λ is the X-ray wavelength (Cu Kα, 0.15406 nm), β is the full width at half maximum (FWHM) of the (101) peak in radians, θ is the Bragg angle corresponding to the (101) reflection at 2θ = 25.2°.Based on this calculation, the average crystallite size of TiO_2 in the composite was found to be approximately 12–18 nm, indicating nanoscale crystallinity consistent with sol–gel synthesized materials.Additionally, the XRD pattern of the CNTs shows a distinct peak at 2θ ≈ 42.1°, corresponding to the (200) plane of graphitic carbon, confirming the presence of well-structured carbon nanotubes within the composite. The broadness of the peak also suggests a degree of structural disorder typical of functionalized CNTs.These results demonstrate the successful incorporation of CNTs and the formation of nanoscaleanataseTiO_2, both critical to the photocatalytic performance of the nanocomposite[27].

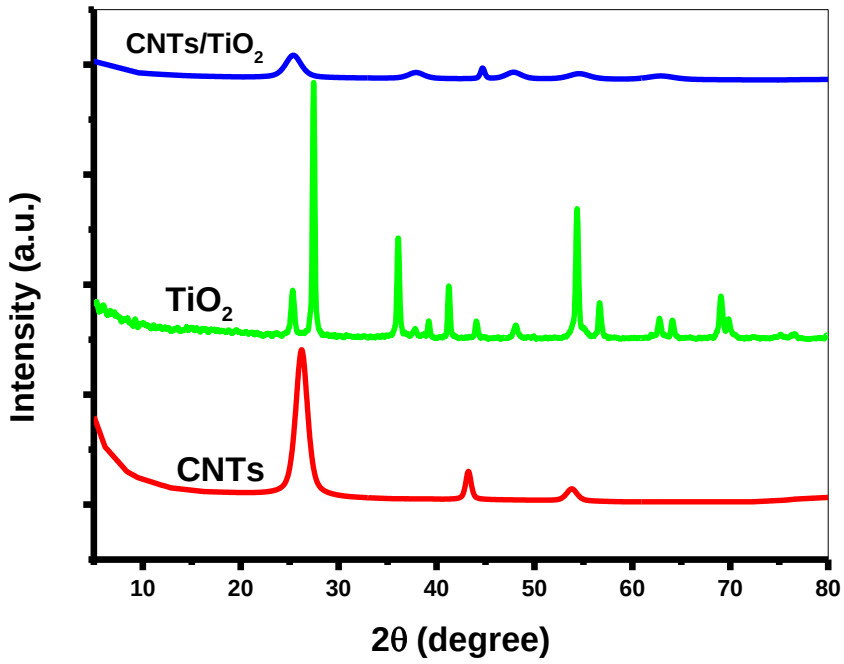

Figure (1) :X-ray diffraction patterns of purified CNTs, calcined pure TiO_2 and CNTs/TiO_2.

4.2. Transmission Electron Microscopy (TEM)

Transmission electron microscopy (TEM) analysis was performed to investigate the morphology and spatial distribution of TiO_2 nanoparticles within the CNTs/TiO_2 nanocomposites, as shown in Figure 2. The TEM images clearly demonstrate a strong interaction between the TiO_2 nanoparticles and the carbon nanotube network. TiO_2 agglomerates appear embedded within and along the CNT surfaces, confirming the formation of a composite microstructure. CNTs act as a physical framework that restricts the free growth of TiO_2, promoting spatial confinement and offering nucleation sites during the sol–gel hydrolysis process.

However, some degree of TiO_2 nanoparticle aggregation is evident in localized regions. This non-uniform distribution likely results from insufficient steric stabilization during the synthesis, although the CNTs effectively act as scaffolds that limit excessive agglomeration and support TiO_2 dispersion throughout the composite [27].

4.3. Band gap calculation

The UV–visible absorption spectra of the synthesized catalysts are presented in Figure 3. Pure TiO_2 exhibits a strong absorption edge in the ultraviolet region near 280 nm, which corresponds to its wide band gap and limited activity under visible light. Upon incorporating CNTs, a notable redshift in the absorption edge is observed, with absorption peaks shifting to longer wavelengths—approximately 303, 334, 355, and 350 nm for CNTs/TiO_2 composites containing 5%, 10%, 15%, and 20% CNTs, respectively. This redshift indicates an enhancement in visible light absorption, which is attributed to the electronic interaction between TiO_2 and the conductive carbon nanotube network.

The observed shift in the absorption edge can be linked to enhanced charge carrier separation and increased electron mobility facilitated by the CNTs. Acting as electron sinks, CNTs help to suppress recombination of photogenerated electron-hole pairs by accepting and transporting electrons away from the TiO_2 surface. This not only improves photogenerated charge carrier lifetime but also contributes to better photocatalytic efficiency under solar irradiation. The improved light-harvesting ability in the visible region, due to the narrowed band gap, expands the range of usable light and supports higher photocatalytic activity [28].

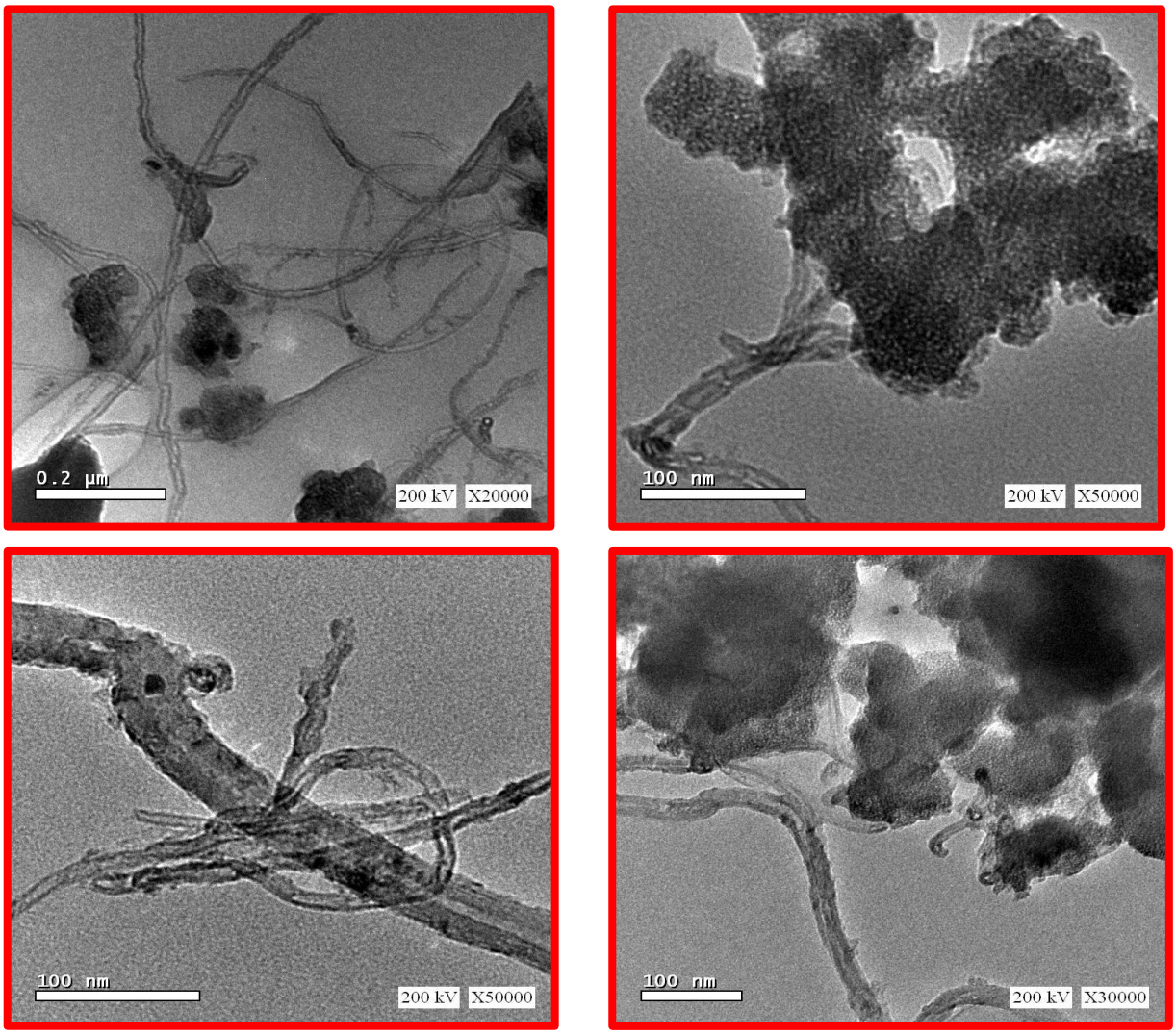

Figure (2):Transmission electron microscope (TEM) of the prepared catalyst CNTs/TiO_2. The arrows point to TiO_2 nanoparticle.

The optical band gap of the materials was estimated using the Tauc relation, shown in Equation (2):

$$\alpha h\upsilon = A(h\upsilon - E_g)^{\frac{n}{2}} \qquad (2)$$

where α is the absorption coefficient, h is Planck's constant, v is the frequency, $E_g$is the band gap energy, A is a proportionality constant, and n is an exponent dependent on the nature of the electronic transition (n = 1 for direct, n = 4 for indirect transitions).

Figure 4 illustrates the Tauc plots for all samples, plotting $(\alpha h\upsilon)^2$ versus photon energy.
The extrapolated intercepts of the linear regions of these curves yielded the estimated band gaps, which are compiled in Table 1. A clear trend of band gap narrowing is evident with increasing CNT content, further confirming the enhanced light absorption and charge transfer interactions between TiO_2 and CNTs.

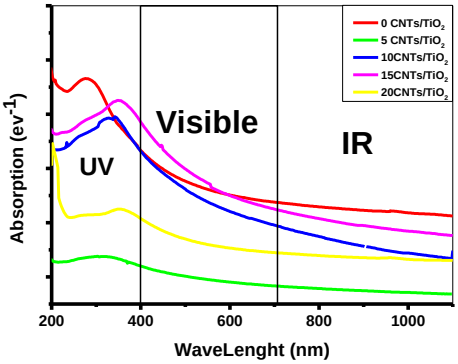

Figure (3): UV–visible absorbance spectra for pure TiO_2 and $CNTs/TiO_2$ (5, 10, 15, 20 Wt%).

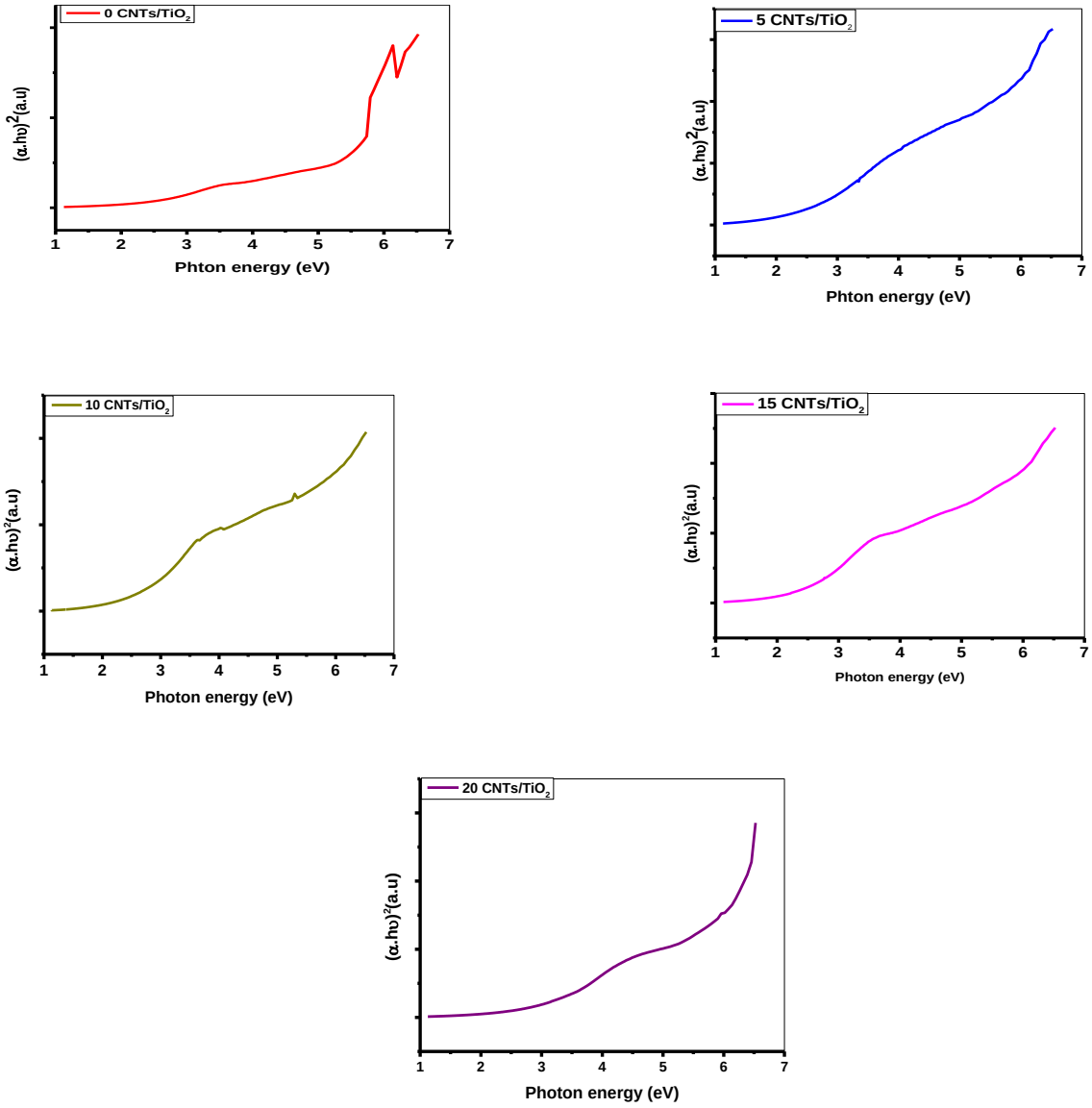

Figure (4): Estimated band gap values of the synthesized catalysts.

Table 1. Estimated band gap energies of CNTs/TiO_2 nanocomposites with varying CNT content, determined using Tauc plot extrapolation based on a direct allowed transition.

CNTs/TiO_2	0	5	10	15	20
Band gap (eV)	2.5	2.4	2.3	2	2.2

4.3. Catalytic Activity: Sunlight-Driven Ammonium Phosphate Hydrolysis

The catalytic performance of the synthesized CNTs/TiO_2 nanocomposites toward the hydrolysis of tri-ammonium phosphate (TAP) under sunlight irradiation is presented in Figure 5. In this study, 1 mmol of TAP in aqueous solution was reacted in the presence of various CNTs/TiO_2 catalysts. The experiments were conducted outdoors under ambient.

Hydrogen evolution volumes were recorded for each catalyst composition, and the results show a clear enhancement with increasing CNT content up to a certain threshold. The measured hydrogen volumes were 23, 25, 27, 35, and 30 mL for composites containing 0%, 5%, 10%, 15%, and 20% CNTs, respectively. The optimal performance was observed at 15% CNT loading. Beyond this concentration, a decline in activity was noted, possibly due to excessive CNT agglomeration and light scattering.

The observed decline in catalytic activity at CNT loadings above 15 wt% is likely due to two main factors. First, excessive CNT content may cause bundling and agglomeration, which can create localized regions of poor dispersion. This not only reduces the number of active TiO_2-CNT interfaces but can also promote charge recombination by limiting effective charge separation. Second, high CNT concentrations may introduce an optical shielding effect, where the dense CNT network absorbs or scatters incident light, thereby reducing the photon flux reaching the TiO_2 surface. This limits the generation of electron-hole pairs necessary for catalytic activity. Furthermore, the pH and ionic strength of the TAP solution were carefully maintained constant across all trials to eliminate variation in hydrolysis kinetics. Since both parameters significantly influence reaction rates and catalyst surface charge, controlling them ensured that the performance differences were attributed solely to the nanocomposite composition and structure.

To ensure reliability, all measurements were performed in triplicate, and the hydrogen volumes are reported as mean values (see Figure 5). The maximum observed enhancement relative to pure TiO_2 was added, confirming the beneficial role of CNT integration.

Several factors contribute to the superior catalytic activity of the CNTs/TiO_2 nanocomposites compared to pure TiO_2: 1.Increased surface area, which improves adsorption of reactants and active species (Yu, Jimmy et al. 2005);2.Heterojunction formation between CNTs and TiO_2, which suppresses recombination of photogenerated charge carriers (Terna, Elemike et al. 2021);3.A positive shift in apparent Fermi level for CNTs/TiO_2 composites relative to pure TiO_2, which enables activation by longer-wavelength light (Kongkanand and Kamat 2007); 4.Photoactivation of CNTs, which inject electrons into the TiO_2 conduction band, facilitating the formation of reactive oxygen species such as superoxide and hydroxyl radicals (van den Berg and Areán 2008).

However, at CNT loadings beyond 15%, reduced activity may result from photon scattering by excess CNTs or insufficient TiO_2 coating, both of which can hinder light absorption and charge transfer efficiency.

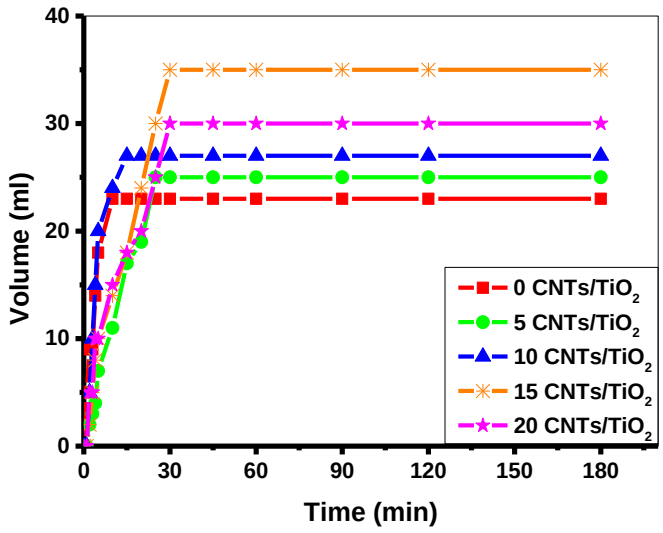

Figure (5): Hydrogen was produced from 1 mmol of TAP using 50 mg of the synthesized catalyst under sunlight at room temperature.

5. Conclusion

In this study, CNTs/TiO_2 nanocomposites with varying carbon content were prepared using the conventional sol–gel strategy. Characterization results confirm that CNTs exert a synergistic effect on the catalytic properties and serve as a stabilizing scaffold for the dispersion of TiO_2 nanoparticles. However, the enhancement in photocatalytic activity was observed only up to an optimal carbon content of 15 wt%. The modest performance improvement is likely linked to the random and heterogeneous distribution of TiO_2 particles along the CNT surfaces, which may limit charge separation efficiency.

Future work could focus on optimizing the dispersion of TiO_2 on CNTs through surface modification or surfactant-assisted methods, evaluating alternative carbon supports (graphene or activated carbon), and assessing the scalability of the synthesis process for practical hydrogen generation applications.

6. Conflicts of interest

"There are no conflicts to declare".

7. Acknowledgment:

This research was funded by the Science, Technology & Innovation Funding Authority (STDF), under the grant (YRG Call 10), project ID(43211).

8. References

1. van den Berg, A.W. and C.O. Areán, *Materials for hydrogen storage: current research trends and perspectives.* Chemical Communications, 2008(6): p. 668-681.
2. Dincer, I., *Green methods for hydrogen production.* International journal of hydrogen energy, 2012. **37**(2): p. 1954-1971.
3. Ganguli, A. and V. Bhatt, *Hydrogen production using advanced reactors by steam methane reforming: a review.* Frontiers in Thermal Engineering, 2023. **3**: p. 1143987.
4. Midilli, A., et al., *A comprehensive review on hydrogen production from coal gasification: Challenges and Opportunities.* International Journal of Hydrogen Energy, 2021. **46**(50): p. 25385-25412.
5. Ren, J.-T., et al., *Water electrolysis for hydrogen production: from hybrid systems to self-powered/catalyzed devices.* Energy & Environmental Science, 2024. **17**(1): p. 49-113.
6. Suárez-Quezada, M., et al., *H2 production by the water splitting reaction using photocatalysts derived from calcined ZnAl LDH.* Fuel, 2019. **240**: p. 262-269.
7. Minero, C. and D. Vione, *A quantitative evalution of the photocatalytic performance of TiO2 slurries.* Applied Catalysis B: Environmental, 2006. **67**(3-4): p. 257-269.
8. Saad, L., et al., *Effect of synthesis approach on characteristics of CZTS kesterite layers for photovoltaic applications.* Egyptian Journal of Chemistry, 2024. **67**(3): p. 425-429.
9. Hamam, L.S., M.S. Abdelaziz Youssef, and E. Ahmed, *Highly Conductive N-type Aluminum Dopped Zinc Oxide for CZTS Kieserite Solar Cell.* Egyptian Journal of Chemistry, 2024. **67**(4): p. 309-313.
10. Yu, H., et al., *TiO2− multiwalled carbon nanotube heterojunction arrays and their charge separation capability.* The Journal of Physical Chemistry C, 2007. **111**(35): p. 12987-12991.
11. Chen, Y., et al., *Preparation of a novel TiO2-based p− n junction nanotube photocatalyst.* Environmental science & technology, 2005. **39**(5): p. 1201-1208.
12. Naffati, N., et al., *Carbon-nanotube/TiO2 materials synthesized by a one-pot oxidation/hydrothermal route for the photocatalytic production of hydrogen from biomass derivatives.* Materials Science in Semiconductor Processing, 2020. **115**: p. 105098.
13. Dai, L., et al., *Carbon-based titanium dioxide materials for hydrogen production in water-methanol reforming: A review.* Journal of Environmental Chemical Engineering, 2022. **10**(2): p. 107326.
14. Gao, B., et al., *Photo-electro-catalysis enhancement on carbon nanotubes/titanium dioxide (CNTs/TiO2) composite prepared by a novel surfactant wrapping sol–gel method.* Applied Catalysis B: Environmental, 2008. **85**(1-2): p. 17-23.
15. Andersson, J. and S. Grönkvist, *Large-scale storage of hydrogen.* International journal of hydrogen energy, 2019. **44**(23): p. 11901-11919.
16. Ensafi, A.A., et al., *Hydrogen storage in hybrid of layered double hydroxides/reduced graphene oxide using spillover mechanism.* Energy, 2016. **99**: p. 103-114.
17. Mohan, M., et al., *Hydrogen storage in carbon materials—A review.* Energy Storage, 2019. **1**(2): p. e35.
18. Li, Y., et al., *Photo-thermal synergic enhancement of CoxFeAl-LDHs for hydrogen generation from hydrolysis of NaBH4.* Applied Surface Science, 2023. **610**: p. 155325.
19. Lim, K.L., et al., *Solid-state materials and methods for hydrogen storage: a critical review.* Chemical Engineering & Technology: Industrial Chemistry-Plant Equipment-Process Engineering-Biotechnology, 2010. **33**(2): p. 213-226.
20. Barakat, N.A., et al., *Ammonium phosphate as promised hydrogen storage material.* international journal of hydrogen energy, 2015. **40**(32): p. 10103-10110.
21. Barakat, N.A., et al., *Ag, Zn and Cd-doped titanium oxide nanofibers as effective photocatalysts for hydrogen extraction from ammonium phosphates.* Journal of Molecular Catalysis A: Chemical, 2015. **409**: p. 117-126.
22. Barakat, N.A., et al., *FexCo1− x-doped titanium oxide nanotubes as effective photocatalysts for hydrogen extraction from ammonium phosphate.* international journal of hydrogen energy, 2018. **43**(16): p. 7990-7997.
23. Barakat, N.A., et al., *Facile synthesis of Ni-incorporated and nitrogen-doped reduced graphene oxide as an effective electrode material for tri (ammonium) phosphate electro-oxidation.* Materials Advances, 2022. **3**(6): p. 2760-2771.
24. Nouruzi, N., et al., *Selective catalytic generation of hydrogen over covalent organic polymer supported Pd nanoparticles (COP-Pd).* Molecular Catalysis, 2020. **493**: p. 111057.
25. Chornaja, S., et al., *Pt supported TiO 2-nanofibers and TiO 2-nanopowder as catalysts for glycerol oxidation.* Reaction Kinetics, Mechanisms and Catalysis, 2016. **119**: p. 569-584.
26. Sheikh, F.A., et al., *Hydrophilically modified poly (vinylidene fluoride) nanofibers incorporating cellulose acetate fabricated by colloidal electrospinning for future tissue-regeneration applications.* Polymer Composites, 2019. **40**(4): p. 1619-1630.
27. Farghali, A.A., et al., *Decoration of multi-walled carbon nanotubes (MWCNTs) with different ferrite nanoparticles and its use as an adsorbent.* Journal of Nanostructure in Chemistry, 2013. **3**: p. 1-12.
28. Mergen, Ö.B. and E. Arda, *Determination of optical band gap energies of CS/MWCNT bio-nanocomposites by Tauc and ASF methods.* Synthetic Metals, 2020. **269**: p. 116539.